“Ionization structure of HII galaxies”

Guillermo Hägele

Enrique Pérez-Montero, Ángeles I. Díaz, Elena Terlevich,
and Roberto Terlevich

Grupo de Astrofísica - UAM / INAOE

Introduction:

- HII galaxies are low mass irregular galaxies with, at least, a recent episode of violent star formation concentrated in a few parsecs close to their cores.

Introduction:

- HII galaxies are low mass irregular galaxies with, at least, a recent episode of violent star formation concentrated in a few parsecs close to their cores.
- The ionizing fluxes originated by these young massive stars dominate the light, the ionization degree and temperature of their interstellar gas.

Introduction:

- HII galaxies are low mass irregular galaxies with, at least, a recent episode of violent star formation concentrated in a few parsecs close to their cores.
- The ionizing fluxes originated by these young massive stars dominate the light, the ionization degree and temperature of their interstellar gas.
- Thus, these systems have an emission line spectrum very similar to those of the extragalactic giant HII regions.

Introduction:

- HII galaxies are low mass irregular galaxies with, at least, a recent episode of violent star formation concentrated in a few parsecs close to their cores.
- The ionizing fluxes originated by these young massive stars dominate the light, the ionization degree and temperature of their interstellar gas.
- Thus, these systems have an emission line spectrum very similar to those of the extragalactic giant HII regions.
- The physical properties of these objects are usually derived combining photoionization model results and observed emission line intensity ratios.

Introduction:

- HII galaxies are low mass irregular galaxies with, at least, a recent episode of violent star formation concentrated in a few parsecs close to their cores.
- The ionizing fluxes originated by these young massive stars dominate the light, the ionization degree and temperature of their interstellar gas.
- Thus, these systems have an emission line spectrum very similar to those of the extragalactic giant HII regions.
- The physical properties of these objects are usually derived combining photoionization model results and observed emission line intensity ratios.
- However, there are several major unsolved problems that limit the confidence of present results, among them:

(1) the effect of temperature structure in multiple-zone models (Pérez-Montero & Díaz 2003, PMD03)

(2) the presence of temperature fluctuations across the nebula (Peimbert 1967, ...)

(3) collisional and density effects on ion temperatures (Luridiana et al. 1999, PMD03)

(4) the ionization structure not adequately reproduced by current models (PMD03)

Observations:

- In order to be able to solve these problems they are needed good quality spectra, with good S/N and spectral range.

Observations:

- In order to be able to solve these problems they are needed good quality spectra, with good S/N and spectral range.

- Our objects were selected from the whole SDSS DR2 spectral catalog using the INAOE Virtual Observatory superserver

Selection criteria: emission line galaxies with EW(Hα) $>$ 50 Å, 1.2 $<$ σ(Hα) $<$ 7 Å, z $<$ 0.2, F(Hα) $>$ 4×10^{-14} erg cm^{-2} s^{-1} Å^{-1}

Observations:

- In order to be able to solve these problems they are needed good quality spectra, with good S/N and spectral range.
- Our objects were selected from the whole DR2 spectral catalog using the INAOE Virtual Observatory superserver

Selection criteria: emission line galaxies with EW(Hα) $>$ 50 Å, 1.2 $<\sigma$(Hα) $<$ 7 Å, z $<$ 0.2, F(Hα) $>$ 4×10^{-14} erg cm^{-2} s^{-1} Å^{-1}

- This preliminary list was processed using BPT (Baldwin, Phillips & Terlevich 1981) diagnostic diagrams in order to remove AGNs (Jesús López, MSc Thesis, INAOE, 2005).

Observations:

- In order to be able to solve these problems they are needed good quality spectra, with good S/N and spectral range.
- Our objects were selected from the whole DR2 spectral catalog using the INAOE Virtual Observatory superserver

Selection criteria: emission line galaxies with EW(Hα) $>$ 50 Å, 1.2 $<\sigma$(Hα) $<$ 7 Å, z $<$ 0.2, F(Hα) $>$ 4 $\times$ 10^{-14} erg cm^{-2} s^{-1} Å^{-1}

- This preliminary list was processed using BPT (Baldwin, Phillips & Terlevich 1981) diagnostic diagrams in order to remove AGNs (Jesús López, MSc Thesis, INAOE, 2005).
- Then, by an independent visual inspection of each object we have selected the final sample.

Observations:

- In order to be able to solve these problems they are needed good quality spectra, with good S/N and spectral range.
- Our objects were selected from the whole DR2 spectral catalog using the INAOE Virtual Observatory superserver

Selection criteria: emission line galaxies with EW(Hα) $>$ 50 Å, 1.2 $<\sigma$(Hα) $<$ 7 Å, z $<$ 0.2, F(Hα) $>$ 4×10^{-14} erg cm^{-2} s^{-1} Å^{-1}

- This preliminary list was processed using BPT (Baldwin, Phillips & Terlevich 1981) diagnostic diagrams in order to remove AGNs (Jesús López, MSc Thesis, INAOE, 2005).
- Then, by an independent visual inspection of each object we have selected the final sample.
- The SDSS spectroscopic data have a resolution (R) of 1800-2100 covering a spectral range from 3800 to 9200 Å, with a single 3” diameter aperture.

Observations:

- In order to be able to solve these problems they are needed good quality spectra, with good S/N and spectral range.
- Our objects were selected from the whole DR2 spectral catalog using the INAOE Virtual Observatory superserver

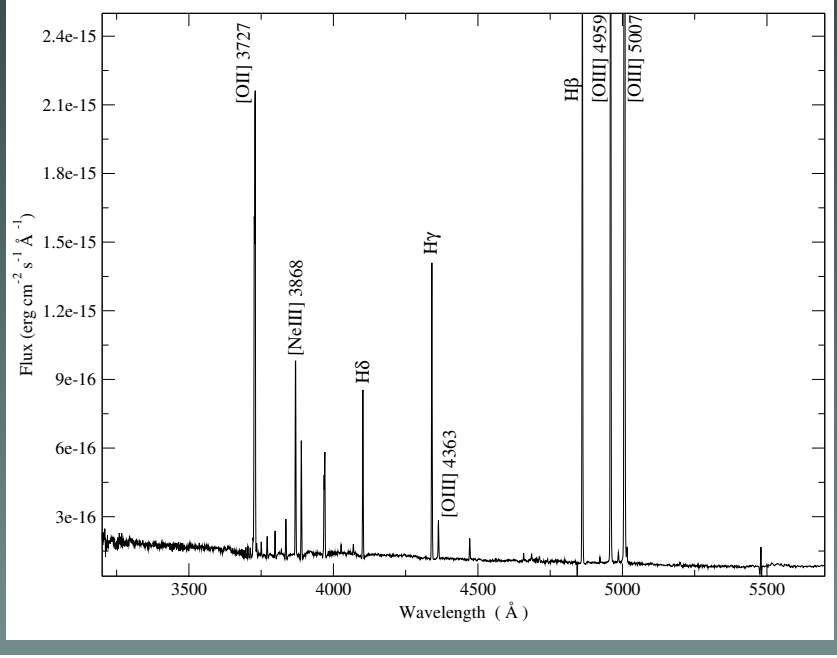
Selection criteria: emission line galaxies with EW(Hα) $>$ 50 Å, 1.2 $<\sigma$(Hα) $<$ 7 Å, z $<$ 0.2, F(Hα) $>$ 4 $\times$ 10^{-14} erg cm^{-2} s^{-1} Å^{-1}

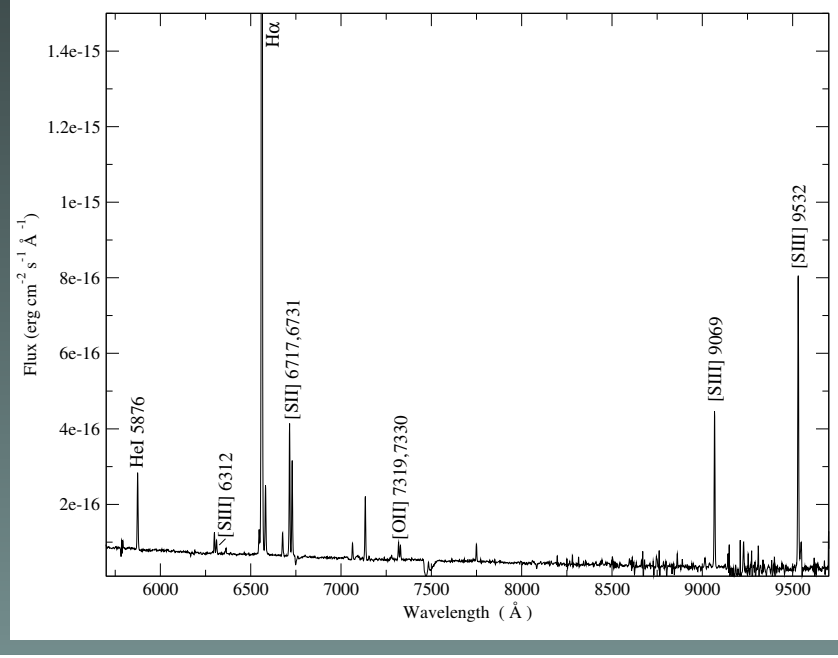
- This preliminary list was processed using BPT (Baldwin, Phillips & Terlevich 1981) diagnostic diagrams in order to remove AGNs (Jesús López, MSc Thesis, INAOE, 2005).
- Then, by an independent visual inspection of each object we have selected the final sample.
- The SDSS spectroscopic data have a resolution (R) of 1800-2100 covering a spectral range from 3800 to 9200 Å, with a single 3" diameter aperture.
- The data were reduced and flux-calibrated using automatic pipelines.

Observations: WHT

- The intermediate resolution blue and far red longslit spectra were obtained simultaneously during an observing run of **one** night using the ISIS double beam spectrograph of the WHT.

	Spectral range	Disp.	FWHM	Spatial res.
blue	3200-5700	0.86Å	2.5Å	0.2”/px
red	5500-10550	1.64Å	4.8Å	0.2”/px

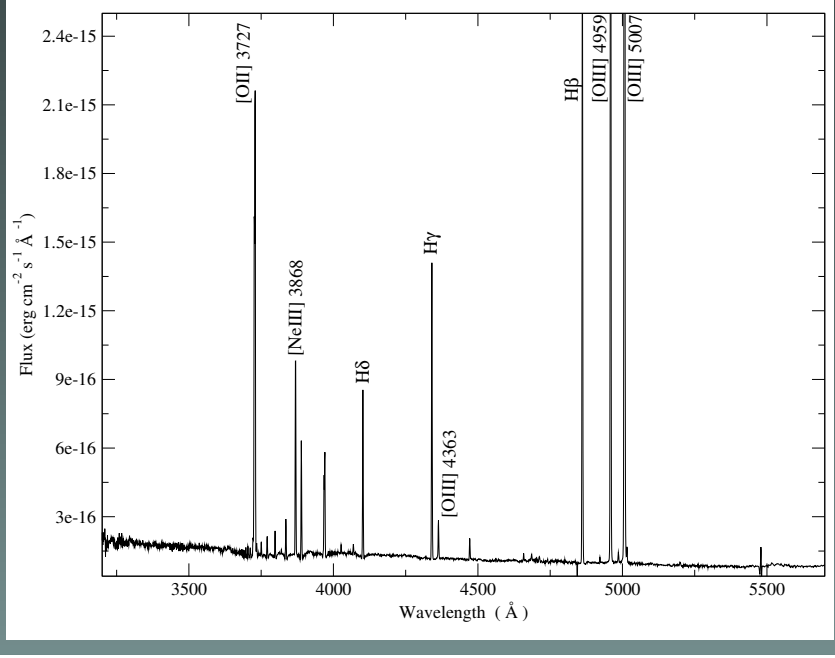


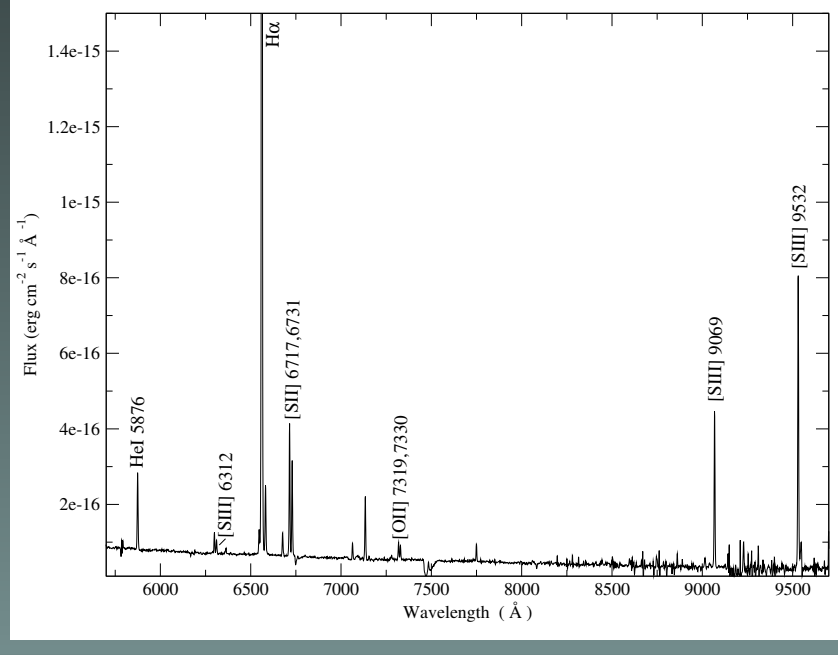


Observations: WHT

- The intermediate resolution blue and far red longslit spectra were obtained simultaneously during an observing run of **one** night using the ISIS double beam spectrograph of the WHT.

- We have chosen the spectral range to measure simultaneously the Balmer discontinuity, and the nebular lines [OII] 3727 and [SIII] 9069, 9532. Moreover, we have measured other important lines such as [OIII] 4363, 4959, 5007, [SII] 4068, 6717, 6731, and [SIII] 6312.





Observations: WHT

- The intermediate resolution blue and far red longslit spectra were obtained simultaneously during an observing run of **one** night using the ISIS double beam spectrograph of the WHT.
- We have chosen the spectral range to measure simultaneously the Balmer discontinuity, and the nebular lines [OII] 3727 and [SIII] 9069, 9532. Moreover, we have measured other important lines such as [OIII] 4363, 4959, 5007, [SII] 4068, 6717, 6731, and [SIII] 6312.
- All the WHT data were reduced using IRAF routines in the usual manner.

Measurements:

- There are some differences between the measurements of the observed fluxes taken with both WHT and SDSS telescopes.

Measurements:

- There are some differences between the measurements of the observed fluxes taken with both WHT and SDSS telescopes.
- A possible explanation of these differences are the different apertures of the WHT and Sloan data, 0.5 and 3”, we are observing different zones of the galaxies.

Measurements:

- There are some differences between the measurements of the observed fluxes taken with both WHT and SDSS telescopes.
- A possible explanation of these differences are the different apertures of the WHT and Sloan data, 0.5 and 3”, we are observing different zones of the galaxies.
- Then, the reddening constant, temperatures, densities and abundances derived using WHT and Sloan data may differ.

Physical conditions:

- Electron temperatures and electron density have been computed from the emission line data using the five-level statistical equilibrium model in the task TEMDEN of IRAF (Pérez-Montero & Díaz 2003).

Physical conditions:

- Electron temperatures and electron density have been computed from the emission line data using the five-level statistical equilibrium model in the task TEMDEN of IRAF (Pérez-Montero & Díaz 2003).
- The emission-line ratios used to calculate each available temperature and density are

Diagnostic	Lines
n([SII])	I(6717Å)/I(6731Å)
T([OIII])	(I(4959Å)+I(5007Å))/I(4363Å)
T([OII])	I(3729Å)/(I(7319Å)+I(7330Å))
T([SIII])	(I(9069Å)+I(9532Å))/I(6312Å)
T([SII])	(I(6717Å)+I(6731Å))/(I(4068Å)+I(4074Å))
T([NII])	(I(6548Å)+I(6584Å))/I(5755Å)

Physical conditions:

- Electron temperatures and electron density have been computed from the emission line data using the five-level statistical equilibrium model in the task TEMDEN of IRAF (Pérez-Montero & Díaz 2003).
- The emission-line ratios used to calculate each available temperature and density are

Diagnostic	Lines
n([SII])	I(6717Å)/I(6731Å)
T([OIII])	(I(4959Å)+I(5007Å))/I(4363Å)
T([OII])	I(3729Å)/(I(7319Å)+I(7330Å))
T([SIII])	(I(9069Å)+I(9532Å))/I(6312Å)
T([SII])	(I(6717Å)+I(6731Å))/(I(4068Å)+I(4074Å))
T([NII])	(I(6548Å)+I(6584Å))/I(5755Å)

- In one of the SDSS spectra (SDSS J003218.59+150014.2) it is not possible to calculate T([OII]).

Physical conditions:

- When we can not measure the lines necessary to estimate a specific temperature we used relationships based on the grids of photoionization models.

SDSS J003218.60+150014.2		
	WHT	SDSS
n([SII])	67:	56:
T([OIII])	1.29±0.02	1.28±0.03
T([OII])	1.47±0.05	—
T([OII])*	1.35±0.02	1.36±0.02
T([SIII])	1.32±0.07	—
T([SIII])*	1.27±0.02	1.27±0.03
T([SII])	0.91±0.04	0.92±0.06
T([NII])	—	—
T([NII])*	1.47±0.05	1.36±0.02

densities in cm^{-3} and temperatures in 10^4 K

Physical conditions:

- When we can not measure the lines necessary to estimate a specific temperature we used relationships based on the grids of photoionization models.

SDSS J162410.11-002202.5		
	WHT	SDSS
n([SII])	56:	66:
T([OIII])	1.24±0.01	1.16±0.01
T([OII])	1.54±0.04	1.23±0.03
T([OII])*	1.33±0.01	1.25±0.01
T([SIII])	1.36±0.05	—
T([SIII])*	1.23±0.01	1.14±0.01
T([SII])	1.12±0.08	1.02±0.09
T([NII])	1.42±0.08	—
T([NII])*	1.52±0.04	1.23±0.02

densities in cm^{-3} and temperatures in 10^4 K

Chemical abundances:

- Ionic and total abundances of He, O, S, N, Ne, Ar and Fe are obtained using the stronger available emission lines detected in the studied spectra.

Chemical abundances:

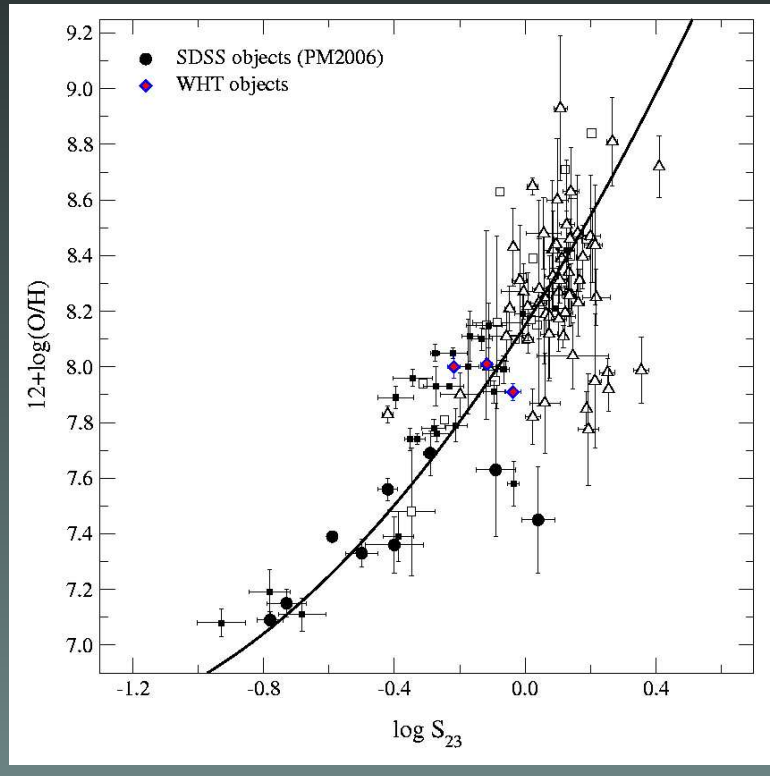
- Ionic and total abundances of He, O, S, N, Ne, Ar and Fe are obtained using the stronger available emission lines detected in the studied spectra.
- Differences between the WHT and SDSS abundances are about 10 % in two cases, and they are in very good agreement, within the observational errors, in the other.

Chemical abundances:

- Ionic and total abundances of He, O, S, N, Ne, Ar and Fe are obtained using the stronger available emission lines detected in the studied spectra.
- Differences between the WHT and SDSS abundances are about 10 % in two cases, and they are in very good agreement, within the observational errors, in the other.

Relation between the S_{23} parameter and the total oxygen abundance in units of 12+log(O/H)

Our three objects are in very good agreement with the empirical calibration (PMD05).



Balmer temperature: T(Bac)

– To measure this value we have adjusted the continuum at both sides of the Balmer discontinuity.

– We can only measure the B-jump in the WHT spectra due to the SDSS spectral range is not appropriate.

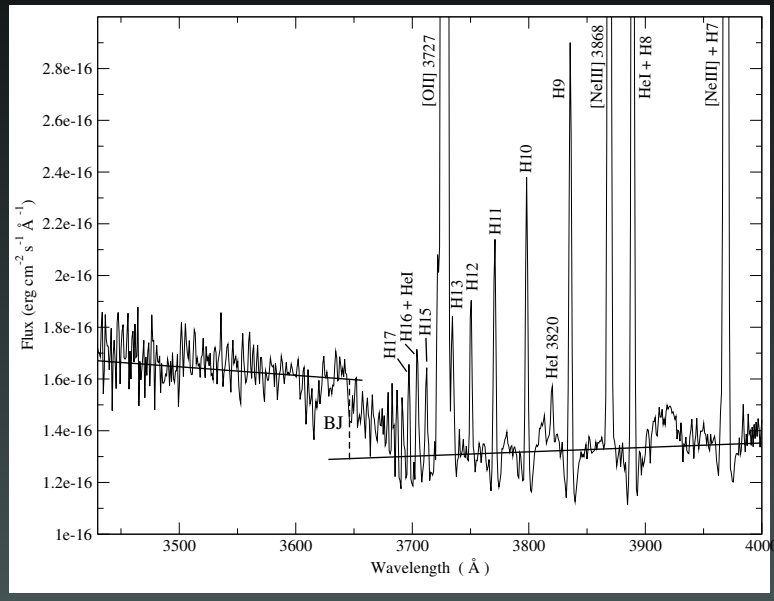
$$T(Bac) = 368 \times (1 + 0.259y^{+} + 3.409y^{++})$$

$$\times \left(\frac{BJ}{H11}\right)^{-3/2} K$$

(Liu et al. 2001)

T([OIII]) = 1.25±0.02; 1.29±0.02; 1.24±0.01

T(Bac) = 1.23±0.27; 0.96±0.16; 1.24±0.27



Balmer temperature: T(Bac)

– To measure this value we have adjusted the continuum at both sides of the Balmer discontinuity.

– We can only measure the B-jump in the WHT spectra due to the SDSS spectral range is not appropriate.

$$T(Bac) = 368\times(1+0.259y^{+}+3.409y^{++})$$

$$\times\left(\frac{BJ}{H11}\right)^{-3/2} K$$

(Liu et al. 2001)

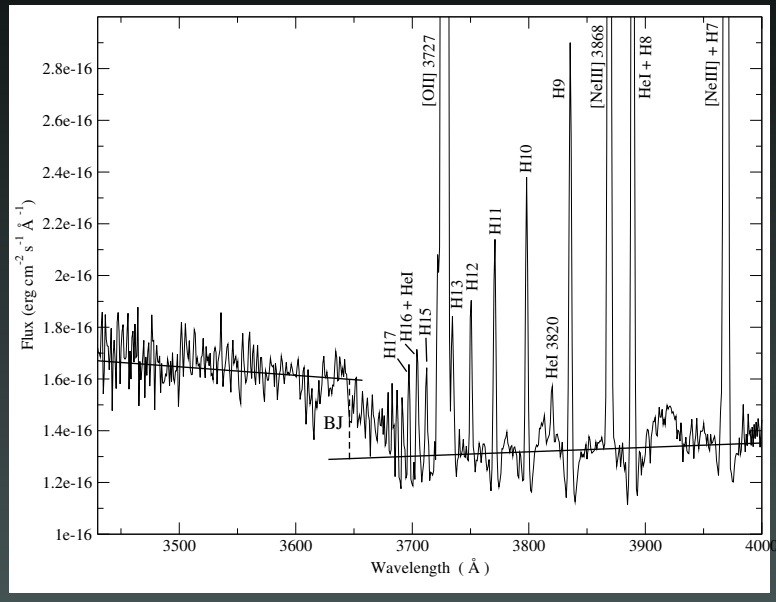
T([OIII]) = 1.25±0.02; 1.29±0.02; 1.24±0.01

T(Bac) = 1.23±0.27; 0.96±0.16; 1.24±0.27

– Assuming a one-ionization scheme:

$$T([OIII]) = T_0\left[1+\frac{1}{2}\left(\frac{91300}{T_0}-3\right)t^2\right]$$

$$T(Bac) = T_0\left(1-1.67t^2\right)$$



Balmer temperature: T(Bac)

– To measure this value we have adjusted the continuum at both sides of the Balmer discontinuity.

– We can only measure the B-jump in the WHT spectra due to the SDSS spectral range is not appropriate.

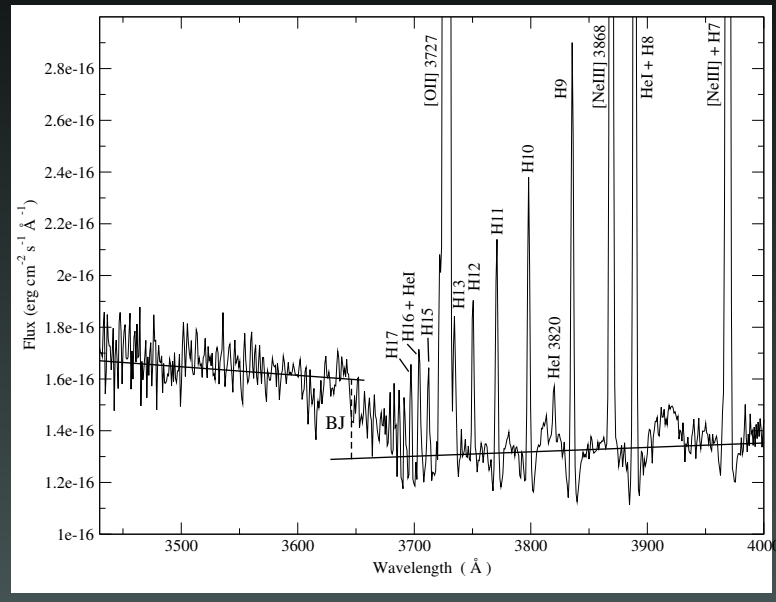
$$T(Bac) = 368\times(1+0.259y^{+}+3.409y^{++})$$

$$\times\left(\frac{BJ}{H11}\right)^{-3/2} K$$

(Liu et al. 2001)

T([OIII]) = 1.25±0.02; 1.29±0.02; 1.24±0.01

T(Bac) = 1.23±0.27; 0.96±0.16; 1.24±0.27



– Assuming a one-ionization scheme:

$$T([OIII]) = T_0\left[1+\frac{1}{2}\left(\frac{91300}{T_0}-3\right)t^2\right]$$

$$T(Bac) = T_0\left(1-1.67t^2\right)$$

Then, the average temperature, T_0, and the root mean square temperature fluctuation, t^2, are

T_0 = 1.24±0.37; 1.08±0.24; 1.24±0.31

$t^2 = 0.005^{+0.045}_{-0.005}$; 0.069±0.029; $0.001^{+0.039}_{-0.001}$

Recalculated chemical abundances:

- We have recalculated the ionic and total abundances taking into account the temperature fluctuations (see work by Peimbert et al.), helped by Jorge García-Rojas and César Esteban, only for the WHT spectra.

Recalculated chemical abundances:

- We have recalculated the ionic and total abundances taking into account the temperature fluctuations (see work by Peimbert et al.), helped by Jorge García-Rojas and César Esteban, only for the WHT spectra.

- There are significant differences only in the case that t^2=0.069, and they are between 0.15 and 0.25 dex.

Preliminary conclusions:

- The spectral range of SDSS can not be extended with new observations since it is very difficult to observe the same region of the galaxies, and the derived physical properties may vary.

Preliminary conclusions:

- The spectral range of SDSS can not be extended with new observations since it is very difficult to observe the same region of the galaxies, and the derived physical properties may vary.
- In some cases the temperature fluctuations could be no negligible, but we need more and better observations to confirm it.

Preliminary conclusions:

- The spectral range of SDSS can not be extended with new observations since it is very difficult to observe the same region of the galaxies, and the derived physical properties may vary.
- In some cases the temperature fluctuations could be no negligible, but we need more and better observations to confirm it.
- We can estimate the temperature fluctuations and the Balmer temperature since our observations have a broad spectral range.

Preliminary conclusions:

- The spectral range of SDSS can not be extended with new observations since it is very difficult to observe the same region of the galaxies, and the derived physical properties may vary.
- In some cases the temperature fluctuations could be no negligible, but we need more and better observations to confirm it.
- We can estimate the temperature fluctuations and the Balmer temperature since our observations have a broad spectral range.
- We need better quality observations to measure the Paschen discontinuity, and, if it is possible, recombination lines, e. g. Carbon, Oxygen or Neon lines.

Preliminary conclusions:

- The spectral range of SDSS can not be extended with new observations since it is very difficult to observe the same region of the galaxies, and the derived physical properties may vary.
- In some cases the temperature fluctuations could be no negligible, but we need more and better observations to confirm it.
- We can estimate the temperature fluctuations and the Balmer temperature since our observations have a broad spectral range.
- We need better quality observations to measure the Paschen discontinuity, and, if it is possible, recombination lines, e. g. Carbon, Oxygen or Neon lines.

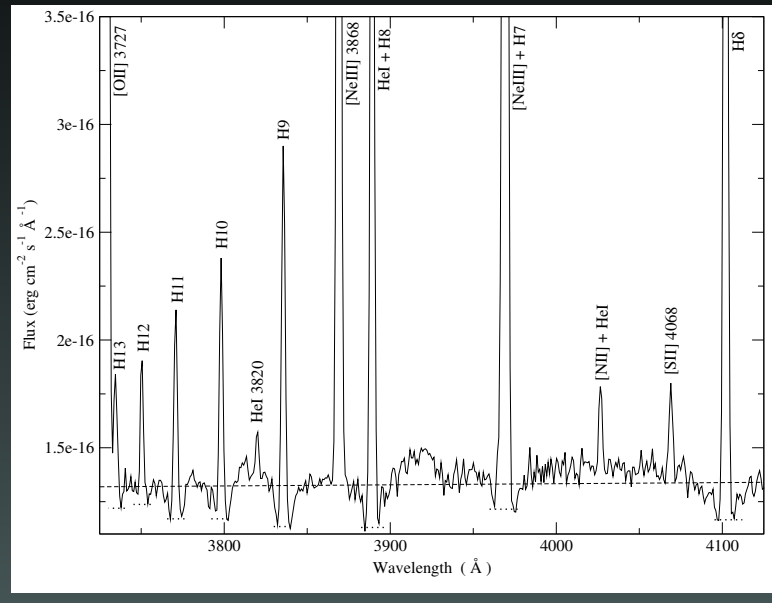
That's all, folks!

Measurements:

– For Balmer and Paschen lines a conspicuous underlying stellar population is easily appreciable by the presence of absorption features that depress the emission lines.

– We have defined a pseudo-continuum to measure these line fluxes.

– The absorbed fractions of the fluxes are not the same for all lines, nore the proportions between the absorbed fractions and the emissions are the same.

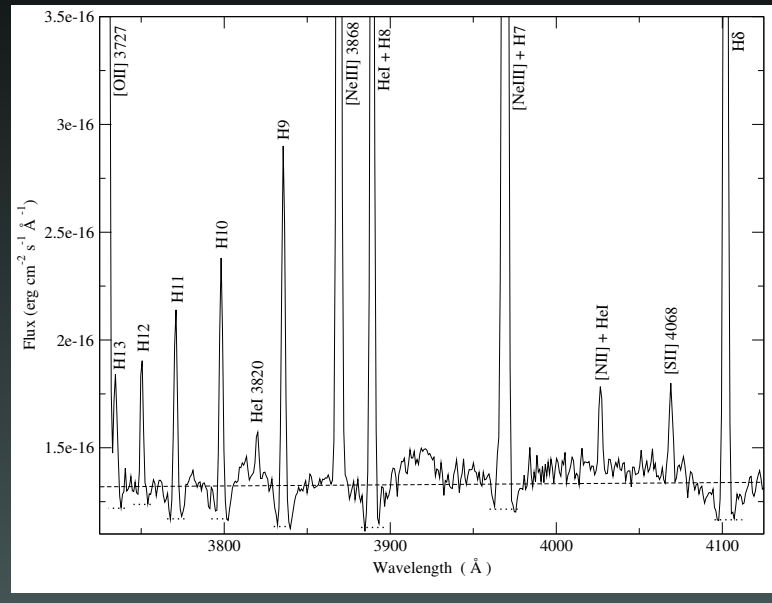


Measurements:

– For Balmer and Paschen lines a conspicuous underlying stellar population is easily appreciable by the presence of absorption features that depress the emission lines.

– We have defined a pseudo-continuum to measure these line fluxes.

– The absorbed fractions of the fluxes are not the same for all lines, nore the proportions between the absorbed fractions and the emissions are the same.



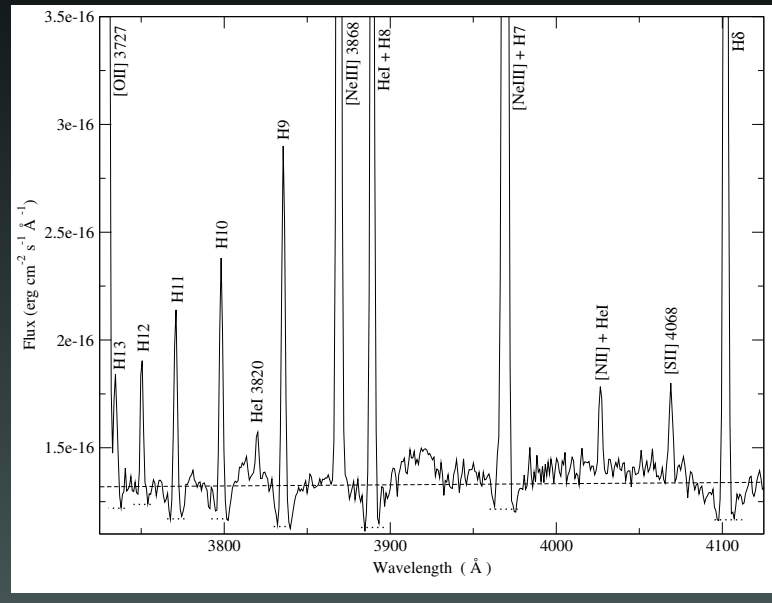
- The fractional errors introduced by this effect on the four strongest Balmer emission lines are much lower than that on the other Balmer lines or the Paschen ones.

Measurements:

– For Balmer and Paschen lines a conspicuous underlying stellar population is easily appreciable by the presence of absorption features that depress the emission lines.

– We have defined a pseudo-continuum to measure these line fluxes.

– The absorbed fractions of the fluxes are not the same for all lines, nore the proportions between the absorbed fractions and the emissions are the same.



- The fractional errors introduced by this effect on the four strongest Balmer emission lines are much lower than that on the other Balmer lines or the Paschen ones.

- Then, C(Hβ) have been calculated using only the four strongest Balmer emission lines (Hα, Hβ, Hγ and Hδ).